

## Comparative study of corrosion inhibition effect of benzodiazepine derivative on the carbon steel surface in 2.0 M H<sub>3</sub>PO<sub>4</sub> and 1.0 M HCl mediums: Electrochemical, theoretical and Monte Carlo simulations studies

T. Laabaissi<sup>1</sup>, H. Lgaz<sup>1</sup>, H. Oudda<sup>1\*</sup>, F. Benhiba<sup>1</sup>, H. Zarrok<sup>1\*</sup>,  
A. Zarrouk<sup>2</sup>, A. El Midaoui<sup>1</sup>, B. Lakhrissi<sup>3</sup>, R. Tourir<sup>4,5</sup>

<sup>1</sup>Laboratoire des procédés de séparation, Faculté des Sciences, Université Ibn Tofail, Kenitra, BP 133, Kenitra, Morocco

<sup>2</sup>LC2AME, Faculty of Sciences, Premier Mohammed University, PO Box 717, 60 000 Oujda, Morocco.

<sup>3</sup>Laboratoire d'Agro ressources et Génie des Procédés, Université Ibn Tofail, Faculté des Sciences, Département de Chimie, B.P. 133, Kénitra, Morocco.

<sup>4</sup>Laboratoire d'Ingénierie des Matériaux et d'Environnement : Modélisation et Application, Faculté des Sciences, Université Ibn Tofail, BP 133, Kénitra 14 000, Morocco.

<sup>5</sup>Centre Régional des Métiers de l'Education et de la Formation (CRMEF), Avenue Allal Al Fassi, Madinat Al Irfane BP 6210 Rabat, Morocco.

Received 14 Nov 2016,  
Revised 20 Dec 2016,  
Accepted 25 Dec 2016

### Keywords

- ✓ HCl;
- ✓ H<sub>3</sub>PO<sub>4</sub>;
- ✓ Benzodiazepine derivative;
- ✓ Corrosion inhibition;
- ✓ Monte Carlo simulations

H. Oudda  
[ouddahassan@gmail.com](mailto:ouddahassan@gmail.com)  
H. Zarrok  
[hzarrok@gmail.com](mailto:hzarrok@gmail.com)

### Abstract

Corrosion inhibition performance of 4,5-benzodiaz-Acetylmethylene-epine-2-one (AMBz) on the corrosion behavior of carbon steel (CS) surface in 2.0 M phosphoric acid and 1.0 M HCl chloridric acid were investigated by analytical methods potentiodynamic polarization and electrochemical impedance spectroscopy and supported by quantum chemical calculation and Monte Carlo (MC) simulation. The inhibition efficiency of AMBz was found to increase with increasing inhibitor concentration but decrease with increasing temperature of both mediums. The IE% reaches 90% and 85% in HCl and phosphoric acid mediums, respectively. Polarization studies showed that this compound was cathodic inhibitor. The inhibition actions of this compound were discussed in view of blocking the electrode surface by means of adsorption of inhibitor molecule obeying Langmuir adsorption isotherm. Thermodynamic parameters of activation were calculated and discussed in depth. Data obtained for inhibition efficiency from the two test techniques are in reasonably good agreement with quantum chemical parameters calculated at DFT/B3LYB/6-31G (d, p) and the Monte Carlo simulation results.

## 1. Introduction

Carbon steel has been extensively used under different conditions in petroleum industries [1]. Aqueous solutions of acids are among the most corrosive media. Acid solutions are widely used in industries for pickling, acid cleaning of boilers, descaling and oil well acidizing [2–9]. Mostly, phosphoric and hydrochloric acids are employed for such purposes [10]. The main problem concerning carbon steel applications is its relatively low corrosion resistance in acidic solutions. Several methods are currently used to prevent corrosion of carbon steel. One such method is the use of an organic inhibitor [2, 7,8]. Effective inhibitors are heterocyclic compounds that have bonds, heteroatom phosphorus, sulfur, oxygen and nitrogen [7–16]. Heterocyclic compounds have been used to inhibit mild steel corrosion in acidic solutions. The efficiency of an inhibitor is largely dependent on its adsorption on the metal surface, which consists of replacement of water molecules by the organic inhibitor at the interface [17,18]. The adsorption of these compounds depends mainly on certain physicochemical properties of the inhibitor molecule such as functional groups, steric factors, aromaticity, electron density at the donor atoms and the electronic structure of the molecules [19,20]. Regarding the adsorption of inhibitor on the metal surface, two types of interactions are

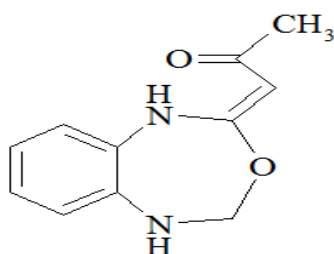
responsible. One is physical adsorption, which involves electrostatic forces between ionic charges or dipoles of the adsorbed species and the electric charge at metal/solution interface. The other is chemical adsorption, which involves charge sharing or charge transfer from inhibitor molecules to the metal surface to form coordinate types of bond [21]. The selection of appropriate inhibitors mainly depends on the type of acid, its concentration, temperature, the presence of dissolved inorganic and/or organic substances even in minor amounts and, of course, on the type of metallic material supposed to be protected [21]. Benzodiazepine molecules shows two anchoring sites available for surface bonding, the nitrogen atom with its lonely sp<sup>2</sup> electron pair and the aromatic rings [10], this type of compounds were used as good corrosion inhibitors [22]. Quantum chemical methods are modern theoretical tools which are widely applied in recent times for the understanding of the complex mechanism of interaction existing between organic molecules adsorbed on a metal surface [23-27]. Density functional theory (DFT) for instance, has been used to predict the molecular geometry, electronic properties and active sites of organic corrosion inhibitors [28]. This could help in the understanding of specific sites of interaction between the inhibitor and the metal surface. On the other hand, Monte Carlo simulation can provide us with information about the low energy adsorption configuration of an organic inhibitor onto a metal surface which cannot be evaluated experimentally [29]. Bensajjay et al. [30] extended their work to study the inhibition effect of 1-phenyl 5-mercaptop 1,2,3,4-tetrazole (PMT) on steel in 0.5 M H<sub>2</sub>SO<sub>4</sub> and 1/3 M H<sub>3</sub>PO<sub>4</sub>, results obtained showed that IE% reached an optimum value of 98% at 10<sup>-3</sup> M PMT.. In other works [31–33], the researchers studied the inhibition effect of red tetrazolium (RT) on the corrosion of cold rolled steel (CRS) in HCl, H<sub>2</sub>SO<sub>4</sub> and H<sub>3</sub>PO<sub>4</sub> solutions. The results show that maximum IE% value of 500 mg L<sup>-1</sup> RT at 20 °C is 94% in 1.0 M HCl [31]; 79%, 1.0 M H<sub>2</sub>SO<sub>4</sub> [32]; and 63%, 3.0 M H<sub>3</sub>PO<sub>4</sub> [33].

This work is devoted to study the inhibition characteristics of 4-Acetylmethylene-1,5-benzodiazepine-2-one (AMBz) for carbon steel in 1.0 M HCl solutions, using potentiodynamic polarization measurements, electrochemical impedance spectroscopy in comparison with our published work [34] studied in 2.0 M H<sub>3</sub>PO<sub>4</sub>. In addition, the quantum chemical studies by DFT method and Monte Carlo simulation were used to elucidate the reactivity of our compound and to well know the unknown properties of investigated Inhibitor in in HCL 1M and H3PO4 2M.

## 2. Experimental details

### 2.1. Inhibitor

All chemicals were purchased from Aldrich or Acros (French). Melting points were determined on an automatic electrothermal IA 9200 digital melting point apparatus in capillary tubes and are uncorrected. <sup>1</sup>H and <sup>13</sup>C NMR spectra were recorded on a Bruker 300 WB spectrometer at 300 MHz for solutions in Me<sub>2</sub>SO-d<sub>6</sub>. Chemical shifts are reported as δ in parts per million (ppm) values with reference to tetramethylsilane (TMS) as internal standard. Infrared spectra were recorded from 400 cm<sup>-1</sup> to 4000 cm<sup>-1</sup> on a Bruker IFS 66v Fourier transform spectrometer using KBr pellets. Mass spectrum was recorded on THERMO Electron DSQ II. More details on the synthesis of 4-Acetylmethylene-1,5-benzodiazepine-2-one (Fig. 1) are presented in our work [34]



**Scheme 1:** 4-Acetylmethylene-1,5-benzodiazepine-2-one (AMBz)

### 2.2. Materials

The steel used in this study is a carbon steel (CS) (Euronorm: C35E carbon steel and US specification: SAE 1035) with a chemical composition (in wt%) of 0.370 % C, 0.230 % Si, 0.680 % Mn, 0.016 % S, 0.077 % Cr, 0.011 % Ti, 0.059 % Ni, 0.009 % Co, 0.160 % Cu and then remainder

iron (Fe). The aggressive solutions of 1.0 M HCl and 2.0 M H<sub>3</sub>PO<sub>4</sub> were prepared by dilution of analytical grade 37% HCl and 85% H<sub>3</sub>PO<sub>4</sub>, respectively, with distilled water. The concentration range of the investigated compound was 10<sup>-3</sup> to 10<sup>-5</sup> M.

### 2.3. Corrosion tests

#### 2.3.1. Electrochemical impedance spectroscopy

The electrochemical measurements were carried out using Volta lab (Tacussel- Radiometer PGZ 100) potentiostat and controlled by Tacussel corrosion analysis software model (Voltmaster 4) at under static condition. The corrosion cell used had three electrodes. The reference electrode was a saturated calomel electrode (SCE). A platinum electrode was used as auxiliary electrode of surface area of 1 cm<sup>2</sup>. The working electrode was carbon steel. All potentials given in this study were referred to this reference electrode. The working electrode was immersed in test solution for 30 minutes to establish steady state open circuit potential (*E*<sub>ocp</sub>). After measuring the *E*<sub>ocp</sub>, the electrochemical measurements were performed. All electrochemical tests have been performed in aerated solutions at 303 K to reach the appropriate conditions of corrosion. The EIS experiments were conducted in the frequency range with high limit of 100 kHz and different low limit 0.1 Hz at open circuit potential, with 10 points per decade, at the rest potential, after 30 min of acid immersion, by applying 10 mV ac voltage peak-to-peak. Nyquist plots were made from these experiments. The best semicircle can be fit through the data points in the Nyquist plot using a non-linear least square fit so as to give the intersections with the *x*-axis.

The inhibition efficiency of the inhibitor was calculated from the charge transfer resistance values using the following equation:

$$\eta_z \% = \frac{R_{ct}^i - R_{ct}^\circ}{R_{ct}^i} \times 100 \quad (1)$$

where,  $R_{ct}^\circ$  and  $R_{ct}^i$  are the charge transfer resistance in absence and in presence of inhibitor, respectively.

#### 2.3.2. Potentiodynamic polarization

The electrochemical behaviour of carbon steel sample in inhibited and uninhibited solution was studied by recording anodic and cathodic potentiodynamic polarization curves. Measurements were performed in the 2.0 MH<sub>3</sub>PO<sub>4</sub> solution containing different concentrations of the tested inhibitor by changing the electrode potential automatically from -900 mV/SCE to -100 mV/SCE at a scan rate of 1 mV s<sup>-1</sup>. The linear Tafel segments of anodic and cathodic curves were extrapolated to corrosion potential to obtain corrosion current densities (*I*<sub>corr</sub>). From the polarization curves obtained, the corrosion current (*I*<sub>corr</sub>) was calculated by curve fitting using the equation:

$$I = I_{corr} \left[ \exp\left(\frac{2.3\Delta E}{\beta_a}\right) - \exp\left(\frac{2.3\Delta E}{\beta_c}\right) \right] \quad (2)$$

$\beta_a$  and  $\beta_c$  are the anodic and cathodic Tafel slopes and  $\Delta E$  is  $E - E_{corr}$ .

The inhibition efficiency was evaluated from the measured *I*<sub>corr</sub> values using the relationship:

$$\eta_{Tafel} \% = \frac{I_{corr}^\circ - I_{corr}^i}{I_{corr}^\circ} \times 100 \quad (3)$$

where  $I_{corr}^\circ$  and  $I_{corr}^i$  are the corrosion current density in absence and presence of inhibitor, respectively.

### 2.4. DFT calculations

Some studies have investigated the correlation between the inhibitor molecular structure and its efficiency. But much less attention has been paid to simulate the adsorption mode of the inhibitor and the metal [35]. The properties include orbital energy, charge density and combined energy, etc. [36]. Quantum chemical calculations were performed using density functional theory (DFT) with the Beck's three parameter exchange functional along with the Lee-Yang-Parr non local correlation functional (B3LYP) [37-39] with 6-31G (d, p) basis set is implemented in Gaussian 03 program electrons ( $\Delta N$  package [40]). This approach is shown to yield favorable geometries for a wide variety of systems. The following quantum chemical parameters were evaluated from the optimized molecular structure: the dipole moment ( $\mu$ ), the energy of the highest occupied molecular orbital ( $E_{HOMO}$ ), the energy of the lowest unoccupied molecular orbital ( $E_{LUMO}$ ), the energy band gap ( $\Delta E_{gap} = E_{HOMO} - E_{LUMO}$ ), the electron affinity (A), the ionization potential (I) and the number of transferred).

### 2.5. Molecular dynamic simulation

The Monte Carlo (MC) search was adopted to compute the low configuration adsorption energy of the interactions of the studied inhibitors on a clean iron surface. The Monte Carlo (MC) simulation was carried out using Materials Studio 6.0 software (Acers, Inc.) [41]. The Fe crystal was cleaved along the (110) plane, it is the most stable surface as reported in the literature [42]. Then, the Fe (110) plane was enlarged to in an appropriate super cell to provide a large surface for the interaction of the inhibitor. The simulation of the interaction between inhibitors and the Fe (110) surface was carried out in a simulation box ( $29.78 \times 29.78 \times 60.13 \text{ \AA}$ ) with periodic boundary conditions, which modeled a representative part of the interface devoid of any arbitrary boundary effects. After that, a vacuum slab with  $50 \text{ \AA}$  thicknesses was built above the Fe (110) plane. All simulations were implemented with the COMPASS force field to optimize the structures of all components of the system of interest. More simulation details on the methodology of Monte Carlo simulations can be found in previous publications [43,44].

## 3. Results and Discussion

### 3.1. Effect of concentration

#### 3.1.1. Tafel Polarization Study

Fig. 2 shows anodic and cathodic polarization plots recorded on mild steel electrode in 1 M HCl in absence and presence of different concentrations of AMBz inhibitor. Electrochemical corrosion parameters, such as corrosion potential  $E_{\text{corr}}$  (mV/SCE), cathodic  $\beta_c$  Tafel slope (mV/dec), the corrosion current density  $I_{\text{corr}}$  ( $\mu\text{A cm}^{-2}$ ) and inhibition efficiency  $\eta_{\text{Tafel}}$  (%) are given in Table 1.

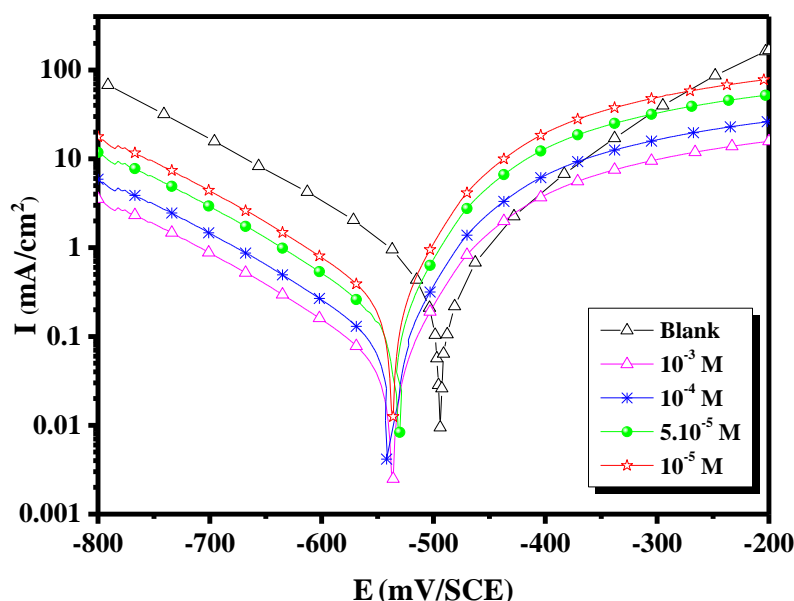


**Figure 2:** Polarization curves of carbon steel in 1.0 M HCl without and with different concentrations of AMBz at 303 K.

From the Fig. 2, it can be seen that the addition of AMBz causes a remarkable decrease in the corrosion rate i.e., shifts the cathodic curves to lower current densities. In other words, both cathodic and anodic reactions of CS electrode are drastically inhibited after the addition of AMBz. This may be ascribed to adsorption of inhibitor over the corroded surface [45]. The cathodic current–potential curves (Fig. 2) give rise to parallel lines indicating that the addition of AMBz to the HCl solutions does not modify the hydrogen evolution mechanism and the reduction of  $\text{H}^+$  ions at the mild steel surface which occurs mainly through a charge transfer mechanism. The inhibitor molecules are first adsorbed onto mild steel surface and blocking the available reaction sites. In this way, the surface area available for  $\text{H}^+$  ions decreases while the actual reaction mechanism remains unaffected [46]. From Table 1, also can find that the corrosion potentials of inhibitor shift slightly in the positive direction for  $\text{H}_3\text{PO}_4$  while in HCl to negative direction. On the other hand, in both mediums, the cathodic Tafel

slope  $\beta_c$  change with insignificant trend in anodic and cathodic directions. From previous results, it can be concluded that tested inhibitor probably act as cathodic inhibitor in HCl and H<sub>3</sub>PO<sub>4</sub> [47]. As it can be seen from Table 1, in both solutions when the concentration of inhibitor increases the inhibition efficiencies increase, while corrosion current densities decrease. The results obtained in both mediums by potentiodynamic polarization confirm the better inhibitive performance of investigated inhibitor.

**Table 1.** Electrochemical parameters and corresponding inhibition efficiency for corrosion of the carbon steel in 1.0 M HCl and 2.0 M H<sub>3</sub>PO<sub>4</sub> in the absence and the presence of different concentrations of AMBz at 303 K.

Medium	Conc (M)	-E <sub>corr</sub> (mV/SCE)	-β <sub>c</sub> (mV/dec)	I <sub>corr</sub> (μA/cm <sup>2</sup> )	η <sub>Tafel</sub> (%)
2.0M H <sub>3</sub> PO <sub>4</sub> [34]	Blank	471	170	2169.1	—
	1×10 <sup>-3</sup>	464	133	0256.0	88.2
	1×10 <sup>-4</sup>	467	140	0501.0	76.9
	5×10 <sup>-5</sup>	472	156	0976.0	55.0
	1×10 <sup>-5</sup>	474	182	1300.0	40.0
1.0M HCl	Blank	496	162	564.0	—
	1×10 <sup>-3</sup>	539	143	64.2	88.62
	1×10 <sup>-4</sup>	542	142	121	78.55
	5×10 <sup>-5</sup>	534	147	182	67.73
	1×10 <sup>-5</sup>	536	152	283	49.82

### 3.1.2. Electrochemical impedance spectroscopy (EIS)

In order to better define the effect of our additive and concentration on the corrosion process, Nyquist plots of mild steel in uninhibited and inhibited acidic solutions containing various concentrations of benzodiazepine derivative are shown in Fig. 3 in 1.0 M HCl. The existence of a single semicircle shows a single charge transfer process during dissolution which is unaffected by the presence of inhibitor molecules. Deviations from perfect circular shape are often referred to the frequency dispersion of interfacial impedance, which arises due to surface roughness, impurities, dislocations, grain boundaries, adsorption of inhibitors, and formation of porous layers and in homogenates of the electrode surface [48,49].

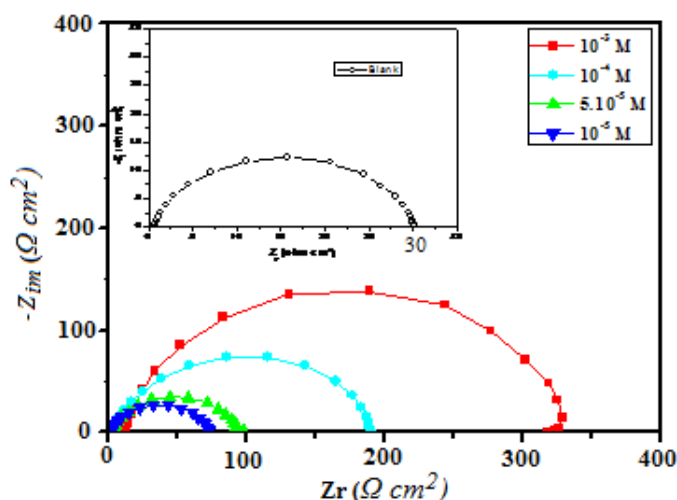


**Figure 3:** Nyquist plots of carbon steel in 1.0M HCl without and with different concentrations of AMBz at 303K

The diameter of the semicircle increases after the addition of AMBz to the aggressive solutions. This increase more and more pronounced with increasing inhibitor concentration. The electrochemical parameters derived from EIS measurements (including, R<sub>ct</sub>, transfer charge, double layer capacitance C<sub>dl</sub> (μF cm<sup>-2</sup>) and the inhibitor efficiency values η<sub>z</sub> (%)) are given in Table 2. Double layer capacitance values were obtained at maximum frequency (f<sub>max</sub>) at which the imaginary component of the Nyquist plot is maximum and calculated using the following equation [50]:

$$C_{dl} = \frac{1}{2\pi f_{\max}} \times \frac{1}{R_{ct}} \quad (4)$$

**Table 2.** Electrochemical impedance parameters and inhibition efficiency for carbon steel in 1.0 M HCl and 2.0 M H<sub>3</sub>PO<sub>4</sub> solution with AMBz at 303K.

Medium	Conc (M)	R <sub>ct</sub> (Ω cm <sup>2</sup> )	C <sub>dl</sub> (μF/cm <sup>2</sup> )	η <sub>z</sub> (%)
H <sub>3</sub> PO <sub>4</sub> [34]	2.0	11.8	118.0	—
	1×10 <sup>-3</sup>	80.5	62.5	<b>85.3</b>
	1×10 <sup>-4</sup>	44.0	72.4	73.2
	5×10 <sup>-5</sup>	25.0	80.6	52.8
	1×10 <sup>-5</sup>	19.5	103.4	39.5
HCl	1.0	29.35	80.18	-
	1×10 <sup>-3</sup>	321.1	11.09	<b>90.86</b>
	1×10 <sup>-4</sup>	188.0	17.05	84.39
	5×10 <sup>-5</sup>	91.41	28.25	67.89
	1×10 <sup>-5</sup>	73.13	68.12	59.86

It is evident from the results collected in Table 2, that AMBz inhibits the corrosion of mild steel in 2 M H<sub>3</sub>PO<sub>4</sub> and 1 M HCl at all the concentrations used, and the inhibition efficiency (η<sub>z</sub>%) increases continuously with increasing concentrations at 303K. *EIS* results (Table 2) show also that the R<sub>ct</sub> values increase and the C<sub>dl</sub> values decrease with increasing the inhibitor concentration. The increase in R<sub>ct</sub> value can be attributed to the formation of protective film on the metal/solution interface [51]. In fact, the decrease in C<sub>dl</sub> values can result from a decrease in local dielectric constant and/or an increase in the thickness of the electrical double layer. It can be assumed that the decrease of C<sub>dl</sub> values is caused by the gradual replacement of water molecules by adsorption of inhibitor molecules on the mild steel surface [52]. On the other hand, the C<sub>dl</sub> of AMBz follow the order of C<sub>dl</sub>(HCl) < C<sub>dl</sub>(H<sub>3</sub>PO<sub>4</sub>), while the R<sub>ct</sub> follow the order of R<sub>ct</sub>(HCl) > R<sub>ct</sub>(H<sub>3</sub>PO<sub>4</sub>), which is an indication that the inhibitive performance of our inhibitor is better in HCl compared with in H<sub>3</sub>PO<sub>4</sub>. The impedance study also gave the same efficiency trend as found in Tafel polarization method.

### 3.2. Effect of temperature

The study of the effect of temperature on the corrosion rate and inhibition efficiency facilitates the calculation of kinetic and thermodynamic parameters for the inhibition and the adsorption processes. These parameters are useful in interpreting the type of adsorption by the inhibitor. To calculate the activation energies and to investigate the mechanism of inhibition of the corrosion process, potentiodynamic polarization measurement (Figs. 4 and 5) was taken at various temperatures in the presence and absence of 10<sup>-3</sup>M of AMBz. The related electrochemical parameters are presented in Table 3.

Table 3 represents the variation of current densities (*I*<sub>corr</sub>) of mild steel corrosion in 1.0 M HCl and 2.0 M H<sub>3</sub>PO<sub>4</sub> in the absence and presence of optimum concentration of the studied compound at different temperature (303–333 K). The results show that *I*<sub>corr</sub> in both mediums increases with increasing solution temperature, while the *IE*% decrease remarkably in the range of the studied temperature for both mediums, which is attributed to increase in the kinetic energy and decrease in the adsorption ability of organic compound at elevated temperature[8].

The activation parameters for the corrosion process were calculated from Arrhenius type plot according to the following equations [9].

$$I_{corr} = k \exp\left(-\frac{E_a}{RT}\right) \quad (5)$$

$$I_{corr} = \frac{RT}{Nh} \exp\left(\frac{\Delta S_a}{R}\right) \exp\left(\frac{\Delta H_a}{RT}\right) \quad (6)$$

Where  $E_a$  is the apparent activation corrosion energy,  $A$  is Arrhenius factor,  $h$  is the Plank's constant,  $N$  is the Avogadro's number, and  $\Delta H$  and  $\Delta S_a$  are the enthalpy and the entropy changes of activation corrosion energies for the transition.  $R$  is the perfect gas constant.

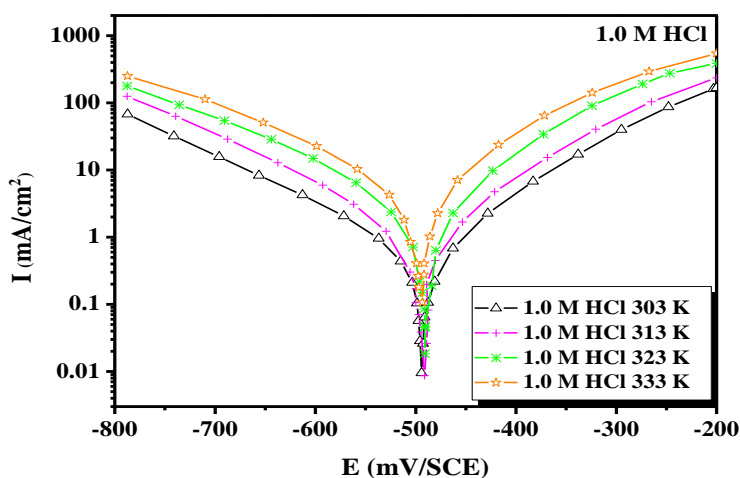


**Figure 4:** Potentiodynamic polarization curves for carbon steel in 1.0 M HCl at different temperatures.

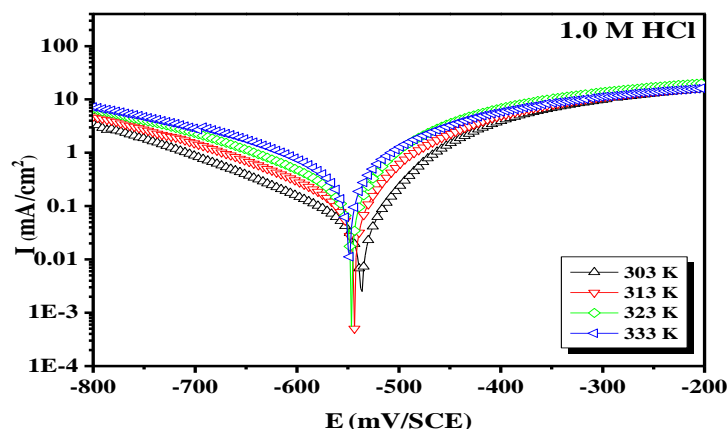


**Figure 5:** Potentiodynamic polarization curves for carbon steel in 1.0 M HCl in the absence and presence of 1.0 mM ABMz at different temperatures.

**Table 3.** Polarization parameters and the corresponding inhibition efficiency for carbon steel in 1.0 M HCl and 2.0 M  $H_3PO_4$  in the absence and presence of 1.0 mM AMBz at different temperatures.

Medium	Temp (K)	$-E_{corr}$ (mV <sub>SCE</sub> )		$I_{corr}$ ( $\mu A cm^{-2}$ )		$\eta_{Tafel}$ (%)	
		$H_3PO_4$	HCl	$H_3PO_4$	HCl	$H_3PO_4$	HCl
Blank	303	418	<b>496</b>	2170	<b>564</b>	—	—
	313	452	<b>498</b>	4910	<b>773</b>	—	—
	323	491	<b>492</b>	6830	<b>1244</b>	—	—
	333	459	<b>497</b>	9390	<b>1650</b>	—	—
AMBz	303	388	<b>539</b>	250	<b>64.2</b>	88.0	<b>88.62</b>
	313	473	<b>546</b>	2183	<b>167</b>	70.0	<b>78.40</b>
	323	479	<b>549</b>	2223	<b>358</b>	55.0	<b>71.22</b>
	333	471	<b>551</b>	4706	<b>641</b>	50.0	<b>61.15</b>

The apparent activation energy was determined from the slopes of  $\ln I_{\text{corr}}$  vs  $1/T$  graph given in Fig. 6. A plot of  $\ln(I_{\text{corr}}/T)$  against  $1/T$  (Fig. 7) gave a straight line with slope  $(\Delta H_a/R)$  and intercept  $(\ln(R/Nh) + (\Delta S_a/R))$ , from which the values of  $\Delta H_a$  and  $\Delta S_a$  were calculated and listed in Table 4.

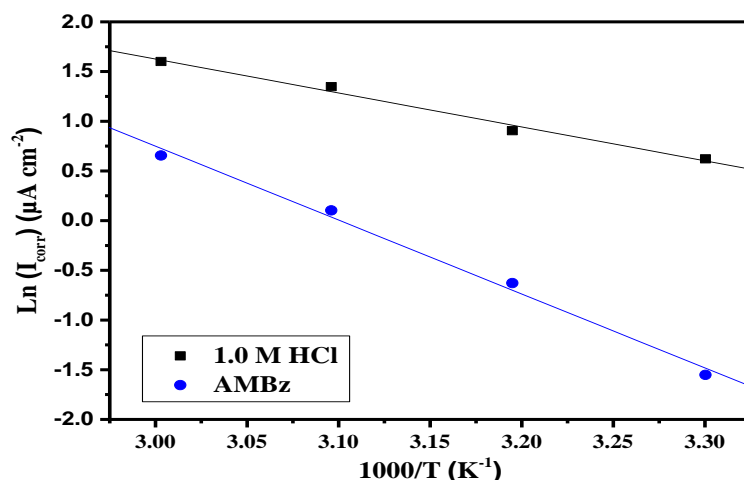


**Figure 6:** Arrhenius plots of carbon steel in 1.0 M HCl with and without 1.0mM of AMBz

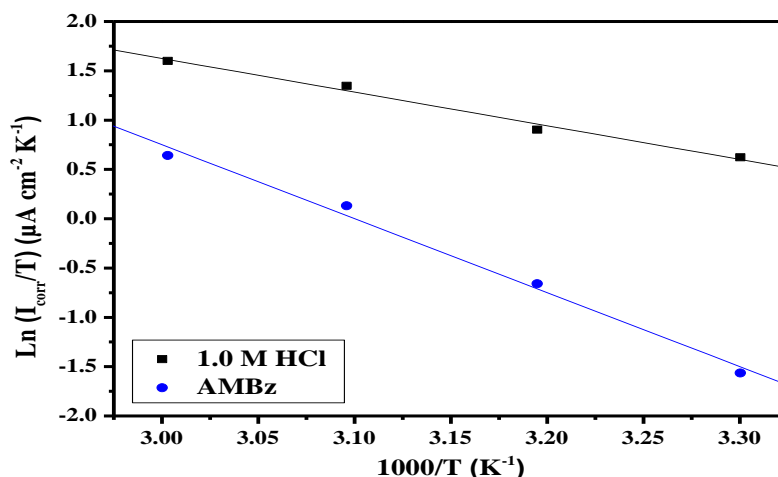


**Figure 7:** Transition Arrhenius plots of carbon steel in 1.0 M HCl with and without 1.0 mM of AMBz.

The increase in activation energy ( $E_a$ ) of inhibited solutions compared to the blank solution suggests that inhibitor is physically adsorbed on the corroding electrode surface, whereas either unchanged or lower energy of activation in the presence of inhibitor suggest chemisorptions [53].

**Table 4.** Activation parameters,  $E_a$ ,  $\Delta H_a$  and  $\Delta S_a$ , of the dissolution of carbon steel in 1.0 M HCl and 2.0 M  $H_3PO_4$  in the absence and the presence of 1.0 mM of AMBz.

Medium	$E_a$ (kJ/mol)	$\Delta H_a$ (kJ/mol)	$\Delta S_a$ (J mol <sup>-1</sup> K <sup>-1</sup> )
2.0 M $H_3PO_4$	39.87	37.23	-57.20
1.0 M HCl	60.79	58.15	-51.84
AMBz + 2.0 M $H_3PO_4$	74.74	72.09	42.61
AMBz + 1.0 M HCl	61.79	59.19	-4.16

As reported in Table 4,  $E_a$  values increased greatly after the addition of the inhibitor. Hence corrosion inhibition of AMBz is primarily occurring through physical adsorption [54]. The positive signs of  $\Delta H_a$  reflected the endothermic nature of the electrode dissolution process. The value of  $\Delta S_a$  is lower for the uninhibited solution than that for the inhibited solution. This phenomenon suggested that a decrease in randomness occurred on going from reactants to the activated complex. The great negative values of entropies indicate that the activated complex in the rate determining step is an association rather than dissociation step meaning that a decrease in disordering takes place on going from reactants to the activated complex [55,56].

### 3.3. Adsorption isotherm

The adsorption isotherm that describes the adsorptive behavior of organic inhibitors is important in order to know the mechanism of corrosion inhibition. Basic information dealing with interaction between the inhibitor molecules and the metal surface can be provided by adsorption isotherms. Several adsorption isotherms were attempted to fit the degree of surface coverage values ( $\theta$ ) to adsorption isotherms including Frumkin, Temkin, Freundlich and Langmuir isotherms. The  $\theta$  values for various concentrations of inhibitors in acidic media have been evaluated from the polarization measurements. The best fit was obtained in the case of Langmuir isotherm which assumes that the solid surface contains a fixed number of adsorption sites and each site holds one adsorbed species [57]. The plot of  $C_{inh}/\theta$  vs.  $C_{inh}$  (Fig. 8) yields a straight line with correlation coefficient of 0.999 for both mediums providing that the adsorption of AMBz on the carbon steel surface obeys Langmuir adsorption isotherm. This isotherm can be represented as [4]:

$$\frac{C_{inh}}{\theta} = \frac{1}{K_{ads}} + C_{inh} \quad (7)$$

where  $C_{inh}$  is the molar concentration of the inhibitor and  $K_{ads}$  is the equilibrium constant for the adsorption-desorption process. The values of  $K_{ads}$  (Table 5) was found to be 44138.61  $M^{-1}$  and 70476.63  $M^{-1}$  in 2.0 M  $H_3PO_4$  and 1.0 M HCl, respectively. The relatively high values of adsorption equilibrium constant reflects the high adsorption ability of AMBz on carbon steel surface [58]. The  $K_{ads}$  is related to the standard free energy of adsorption,  $\Delta G_{ads}^\circ$ , by the following equation[5]:

$$K_{ads} = \left( \frac{1}{55.5} \right) \exp \left( -\frac{\Delta G_{ads}^\circ}{RT} \right) \quad (8)$$

where R is gas constant and T is absolute temperature of experiment and the constant value of 55.5 is the concentration of water in solution in  $mol L^{-1}$ .

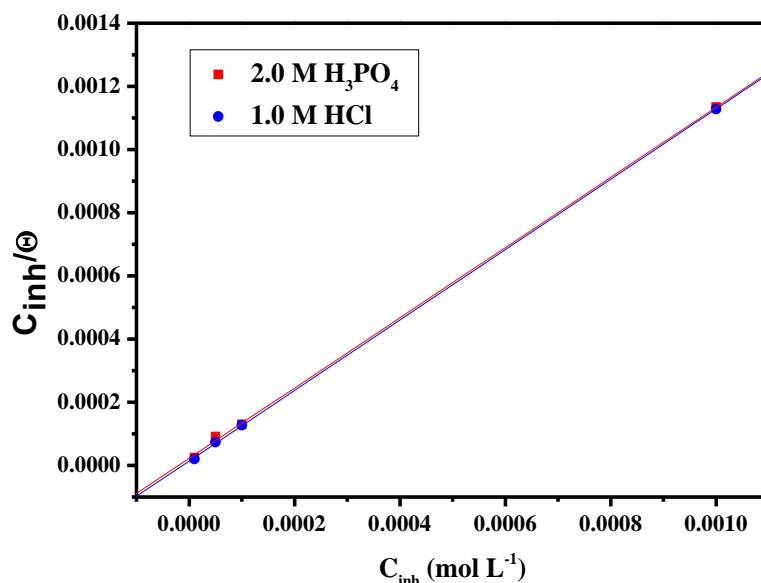


**Figure 8:** Langmuir adsorption isotherm plots for AMBz at 303K.

The  $\Delta G_{ads}^{\circ}$  values were calculated as  $-36.26 \text{ kJ mol}^{-1}$  and  $-38.22 \text{ kJ mol}^{-1}$  in 2.0 M  $\text{H}_3\text{PO}_4$  and 1.0 M  $\text{HCl}$ , respectively. The negative values of  $\Delta G_{ads}^{\circ}$  indicates the spontaneity of the adsorption process and the stability of adsorbed layer on the carbon steel surface. It is well known that the values of  $\Delta G_{ads}^{\circ}$  of the order of  $-20 \text{ kJ mol}^{-1}$  or lower indicate a physisorption; those of order of  $-40 \text{ kJ mol}^{-1}$  or higher involve charge sharing or transfer from the inhibitor molecules to the metal surface to form a coordinate type of bond (chemisorption) [59-61]. On the other hand, the adsorption phenomenon of an organic molecule is not considered only as a purely physical or chemical adsorption phenomenon [62,63]. A wide spectrum of conditions, ranging from the dominance of chemisorption or electrostatic effects, arises from other adsorptions experimental data [64]. The values of  $\Delta G_{ads}$  may suggest both chemisorption and physisorption modes. It can be observed that the adsorption of our inhibitor occur by same mechanism in both mediums.

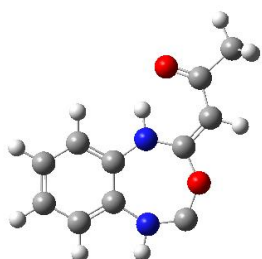
**Table 5.** Adsorption parameters of AMBz for mild steel corrosion in 2.0 M  $\text{H}_3\text{PO}_4$  and 1.0 M  $\text{HCl}$  at 303 K.

Medium	$R^2$	$K_{ads}(\text{M}^{-1})$	$\Delta G_{ads}^{\circ}$ (KJ/mol)
2.0 M $\text{H}_3\text{PO}_4$	0.99	44138.61	-36.26
1.0 M $\text{HCl}$	0.99	70476.63	-38.22

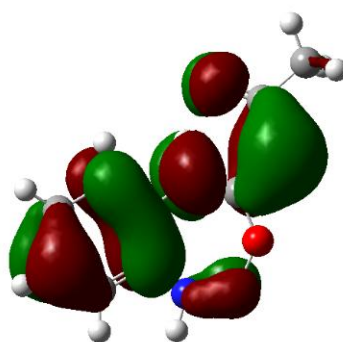
### 3.4. Quantum chemical calculations

In order to study the effect of molecular structure on the inhibition efficiency, quantum chemical calculations were performed by using DFT and all the calculations were carried out with the help of complete geometry optimization. The optimized geometry, EHOMO and ELUMO of AMBz in gaseous media are shown in Fig. 9.

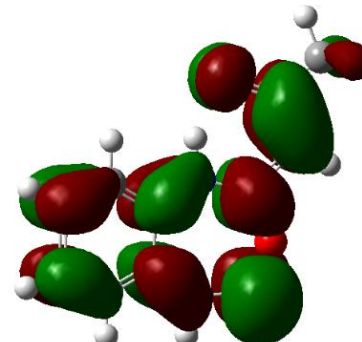
**Optimized molecular structure**



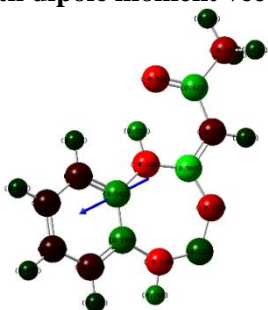
**HOMO**



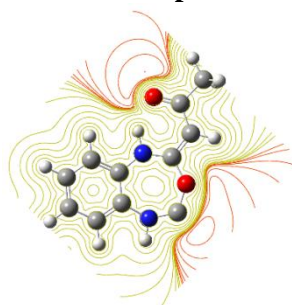
**LUMO**



**Mulliken charge distribution with dipole moment vector**



**Contour of molecular electrostatic potential**



**Molecular electrostatic potential mapped**

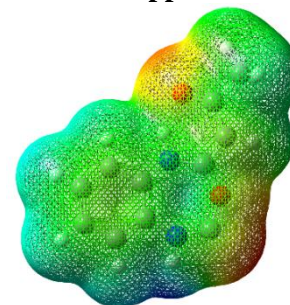


**Figure 9:** Optimized structure, frontier molecular orbital density distributions, Mulliken charges with dipole moment and electrostatic properties of AMBz.

As per the frontier molecular orbital theory, frontier molecular orbital's HOMO and LUMO are involved in the course of adsorption of the inhibitor molecules [65]. In general the higher the value of HOMO, the higher would be the electron donating capacity of the inhibitor to vacant d-orbital of the metal. In addition, the lower the value

of LUMO, the greater would be the electron accepting ability of the inhibitor from the filled metal orbitals. But, the most important parameter is  $\Delta E$ , which is the energy difference between LUMO and HOMO. The lower the value of  $\Delta E$  the easier would be the release of electron and the stronger would be the adsorption [66]. Thus to become a good corrosion inhibitor, easy donation of electron as well as easy acceptance of electron in their vacant orbital's is necessary [67]. The quantum chemical parameters for AMBz in gaseous media are represented in Table 6.

**Table 6.** Quantum theoretical parameters for AMBz calculated using B3LYP/6-31G (d, p)

$E_{\text{HOMO}}$	$E_{\text{LUMO}}$	$\Delta E$	I	A	$\omega$	$\Delta N$	$\mu$
-5.7870	-1.7733	4.013	5.7870	1.7733	14.3388	0.802	2.5272

From this table, low values of the dipole moment ( $\mu$ ) will favor the accumulation of inhibitor molecules on the metallic surface [68].

The number of electron transfer ( $\Delta N$ ) was calculated using the following equation [69]:

$$\Delta N = \frac{\phi - \chi_{inh}}{2(\eta_{Fe} + \eta_{inh})} \quad (9)$$

Where  $\chi_{Fe}$  and  $\chi_{inh}$  denote the absolute electro negativity of Fe and the inhibitor molecule, respectively;  $\eta_{Fe}$  and  $\eta_{inh}$  are the absolute hardness of mild steel and the inhibitor molecule, respectively. The above quantum chemical parameters are related to electron affinity (A) and ionization potential (I) [70].

$$\chi = \frac{I - A}{2} \quad \text{and} \quad \eta = \frac{I + A}{2} \quad (10)$$

Where  $I = -E_{\text{HOMO}}$  and  $A = -E_{\text{LUMO}}$ .

$\chi$  and  $\eta$  are calculated using the values of I and A. The theoretical values of  $\phi$  and  $\eta$  of Fe are 3.91 eV and 0 eV, respectively. According to Lukovits et al [71]. If the value of  $\Delta N$  is less than 3.6, the efficiency of inhibition increases with increasing electron-donating ability of the inhibitor to the metal surface. Recently, Parr et al. [72], have introduced an electrophilicity index ( $\omega$ ) defined as:

$$\omega = \frac{\chi^2}{2\eta} \quad (11)$$

This was proposed as a measure of the electrophilic power of a molecule. Molecule with higher value of  $\omega$  has the higher capacity to accept electrons. The Mulliken atomic charges on the atoms of the studied molecules with optimized geometry and the direction of the dipole moment vector calculated at the B3LYP/6-31G(d,p) level are presented in Fig. 9. It is clear from this figure, that all the nitrogen atoms as well as oxygen atoms and some carbons atoms carries negative charge centers which are the probable reactive sites, could offer electrons to the mild steel surface to form a coordinate bond. It is worthy to mention that there are more negative charge centers in AMBz. The contour and is surface representation of electrostatic potential are also presented in Fig.9. The different values of the electrostatic potential were demonstrated with the help of different colors which are red, yellow, green, light blue and blue. The red and yellow colors suitable for the negative parts of the MESP are linked to electrophilic reactivity, blue colors suitable for the positive parts to the nucleophilic reactivity and the green color represents the electrostatic potential zero region [73]. According to the ESP contour surface and MESP of studied inhibitor, the negative regions are electrophilic active regions are mainly observed over the oxygen atoms. The positive regions are the nucleophilic regions and these are over the some carbon atoms of the title molecule.

### 3.5. Monte Carlo simulation

Electronic properties alone are not sufficient to predict the trend of the inhibition performance of the investigated inhibitors in spite of its success in exploring the mechanism of inhibitors. Therefore, it is imperative to carry out rigorous modeling of the direct interaction of the inhibitors with steel. We carried out Metropolis Monte Carlo method to sample possible low energy searches of the configuration space of the inhibitor on clean iron surface. The most stable low energy adsorption configurations of the inhibitor on Fe (110) surface using Monte Carlo simulations are depicted in Fig. 10. The values for the outputs and descriptors of the Monte Carlo simulations are listed in Table 7. It is generally acknowledged that the primary mechanism of corrosion inhibitor

interaction with steel is by adsorption. So the adsorption energy can provide us with a direct tool to rank inhibitor molecules. The adsorption energy of AMBz is far higher (Table 7). This indicates the possibility of gradual substitution of water molecules from the iron surface resulting in the formation of a stable layer which can protect the iron from aqueous corrosion [74-76].

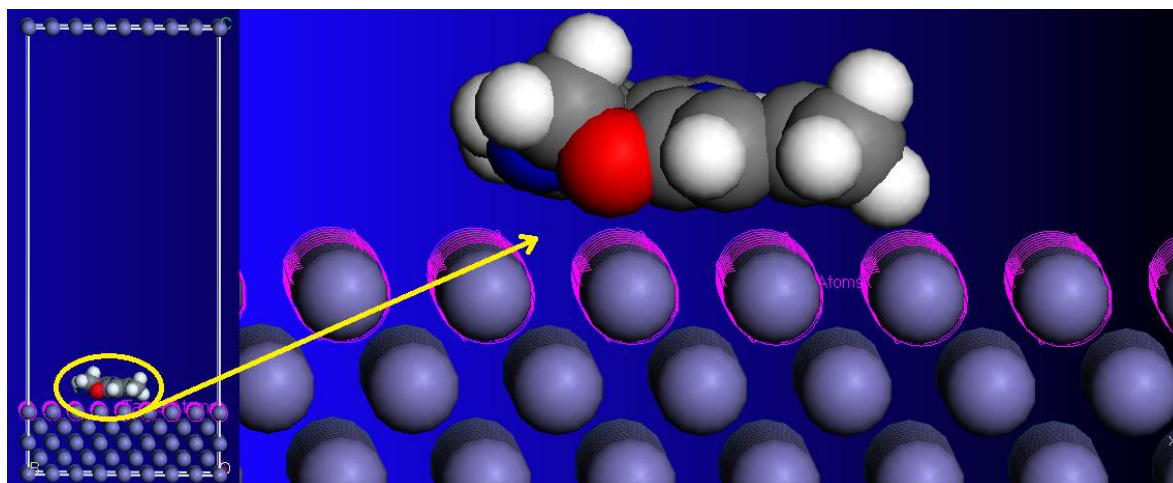


**Figure 13:** The most stable low energy configuration for the adsorption of the inhibitor on Fe (1 1 0) surface obtained through the Monte Carlo simulation.

**Table 7.** Outputs and descriptors calculated by the Monte Carlo simulation for the lowest adsorption. Configurations of DHI Fe (110) surface (in kcal/mol).

System	Total Energy	Adsorption energy	Rigid adsorption energy	Deformation energy	dEad/dNi inhibitor
Fe (1 1 0)/AMBz	200.49	-100.20	-99.49	-0.70	-100.20

## Conclusions

The corrosion inhibition of carbon steel in 1.0 M HCl solutions by AMBz was studied and compared with the results obtained in 2.0 M H<sub>3</sub>PO<sub>4</sub> [28] using common electrochemical techniques and quantum chemical calculations by DFT method and Monte Carlo simulations for the study of AMBz. According to experimental and theoretical findings, it could be concluded that:

- AMBz is a good corrosion inhibitor for the carbon steel protection in both acid solutions. The inhibitory efficiency of this compound depends on its concentration in both acid solutions.
- EIS plots indicated that  $R_{ct}$  values increase and  $C_{dl}$  values decrease with increasing inhibitor concentration.
- Polarization curves indicated that AMBz act as cathodic type inhibitor.
- The adsorption of AMBz on the steel surface from two acid solutions follows Langmuir adsorption isotherm. The thermodynamic parameters suggest that this inhibitor is strongly adsorbed on the carbon steel surface.
- The quantum chemical parameters (such as  $E_{HOMO}$ ,  $E_{LUMO}$ , and dipolar moment) are obtained and discussed in view of experimental results.
- Both experimental, quantum chemical and Monte Carlo simulations results showed that the inhibition efficiency of AMBz is affected by the heteroatoms and  $\pi$ -system presented in our compound.

## References

1. Saadouni M., Larouj M., Salghi R., Lgaz H., Jodeh S, Zougagh M, and, Souizi A., *Der Pharm. Lett.* 8 (4) (2016) 65.
2. Saadouni M., Larouj M., SalghiR., Lgaz H., Jodeh S, Zougagh M and Souizi A., *Der Pharm. Lett.* 8 (4) (2016) 96.

3. Larouj M., Lgaz H., Zarrok H., Serrar H., Zarrok H., Bourazmi H., Zarrouk A., Elmidaoui A., Guenbour A., Boukhris S and Oudda H., *J. Mater. Environ. Sci.* 6 (11) (2015) 3251.
4. Larouj M., Belkhaouda M., Lgaz H., Salghi R., Jodeh S., Samhan S., Serrar H., Boukhris S., Zougagh M and Oudda H., *Der Pharm. Chem.* 8(2) (2016) 114.
5. Lgaz H., Benali O., Salghi R., Jodeh S., Larouj M., Hamed O., Messali M., Samhan S., Zougagh M and Oudda H., *Der Pharm. Chem.* 8(2) (2016) 172.
6. Afia L., Larouj M., Lgaz H., Salghi R., Jodeh S., Samhan S and Zougagh M., *Der Pharm. Chem.* 8(2) (2016) 22.
7. Lgaz H., ELaoufir Y., Ramli Y., Larouj M., Zarrok H., Salghi R., Zarrouk A., Elmidaoui A., Guenbour A., Essassi EL M., Oudda H., *Der Pharm. Chem.* 7(6) (2015) 36.
8. EL Makrini B., Larouj M., Lgaz H., Salghi R., Salman A., Belkhaouda M., Jodeh S., Zougagh M., Oudda H., *Der Pharm. Chem.* 8(2) (2016) 227.
9. Makrini EL B., Lgaz H., Larouj M., Salghi R., Rasem Hasan A., Belkhaouda M., Jodeh S., Zougagh M., Oudda H., *Der Pharm. Chem.* 8(2) (2016) 256.
10. Khalifa M A., El-Batouti EL M., Mahgoub F., Bakr Aknish A., *Mater. Corros.* 54 (2003) 251.
11. Zarrok H., Oudda H., El Midaoui A., Zarrouk A., Hammouti B., Ebn Touhami M., Attayibat A., Radi S., Touzani R., *Res. Chem. Intermed.*, 38 (2012) 2051.
12. Zarrouk A., Hammouti B., Zarrok H., Bouachrine M., Khaled K.F., Al-Deyab S.S., *Int. J. Electrochem. Sci.*, 6 (2012) 89.
13. Zarrouk A., Hammouti B., Dafali A., Zarrok H., *Der Pharm. Chem.*, 3 (2011) 266.
14. Zarrok H., Zarrouk A., Salghi R., Oudda H., Hammouti B., Assouag M., Taleb M., Ebn Touhami M., Bouachrine M., Boukhris S., *J. Chem. Pharm. Res.*, 4 (2012) 5056.
15. Ghazoui A., Zarrouk A., Bencaht N., Salghi R., Assouag M., El Hezzat M., Guenbour A., Hammouti B., *J. Chem. Pharm. Res.*, 6 (2014) 704.
16. Zarrok H., Zarrouk A., Salghi R., Assouag M., Hammouti B., Oudda H., Boukhris S., Al Deyab S.S., Warad I., *Der Pharm. Lett.*, 5 (2013) 43.
17. Abboud Y., Abourriche A., Saffaj T., Berrada M., Charrouf M., Bennamara A., Himidi ALN., Hannache H., *Mater. Chem. Phys.* 105 (2007) 1.
18. Wang H., Fan H., Zheng J., *Mater. Chem. Phys.* 77 (2002) 655.
19. Khaled F. K., *Electrochim. Acta* 48 (2003) 2493.
20. Popova A., Christov M., Raicheva S., *Sokolova.E, Corros. Sci.* 46 (2004) 1333.
21. Noor A. E., Al-Moubaraki H. A., *Mater. Chem. Phys.* 110 (2008) 145.
22. Niouri W., Zerga B., Sfaira M., Taleb M., Ebn Touhami M., Hammouti B., Essassi E. M., *Int. J. Electrochem. Sci.* 9 (2014) 8283.
23. John S., Kuruvilla M., Joseph A., *RSC Adv.* 3 (2013) 8929.
24. Kabanda M.M., Obot B.I., Ebenso E.E., *Int. J. Electrochem. Sci.* 8 (2013) 10839.
25. Obot B.I., Obi-Egbedi O.N., *Corros. Sci.* 52 (2010) 657.
26. Khaled F.K., *J. Chim. Acta* 1 (2012) 66.
27. Guo L., Zhu S., Zhang S., Q He., W. Li, *Corros. Sci.* 87 (2014) 366.
28. Fu J., Li S., Wang Y., Liu X., Lu L., *J. Mater. Sci.* 46 (2011) 3550.
29. Khaled F.K., *J. Chim. Acta* 1 (2012) 59.
30. Bensajjay E., Alehyen S., El Achouri M., Kertit S., *Anti-Corros. Meth. Mater.* 50 (2003).
31. Li X H., Deng S D., Fu H., *Chin. J. Appl. Chem.*, 26 (2009) 1075 (in Chinese).
32. Li X H., Deng S D., Fu H., *Corros. Sci.* 51 (2009) 1344.
33. Li X H., Deng S D., Fu H., *Mater. Chem. Phys.* 115 (2009) 815.
34. Laabaissi T., Bouassiria M., Oudda H., Zarrok H., Zarrouk A., Elmidaoui A., Lakhrissi L., Lakhrissi B., El Essassi M., Tourir R., *J. Mater. Environ. Sci.* 7 (5) (2016) 1538.
35. Khalil N., *Electrochim Acta* 48 (2003) 2635.
36. M Özcan., İ Dehri., M Erbil., *Appl. Surf. Sci.* 236 (2004) 155.
37. Becke D A., *Chem. Phys.J.* 96 (1992) 2155.
38. Becke D.A., *Chem. Phys.J.* 98 (1993) 5648.
39. C Lee., W Yang., Robert G Parr., *Phys. Rev. B.* 37 (1988) 785.
40. Frisch M J., et al., *GAUSSIAN 03, Revision B.03, Gaussian, Inc., Wallingford, CT, 2004.*
41. Materials Studio., *Revision 6.0. Accelrys Inc., San Diego, USA 2013.*
42. Verma C., Ebenso E.E., Bahadur I., Obot I.B., Quraishi A.M., *J. Mol. Liq.* 212(2015) 209.

43. Musa Y.A., Jalgham T.R., Mohamad B.A., *Corros. Sci.* 56 (2012) 176.
44. Kaya S., Tüzün B., Kaya C., et Obot B.I., *J. Taiwan Inst. Chem. Eng.* 58 (2016) 528.
45. Shukla K.S., Quraishi A.M., *Corros. Sci.* 52 (2010) 314.
46. Shukla K.S., Quraishi M.A., *Corros. Sci.*, 51 (2009) 1990.
47. Bentiss F., Traisnel M., Lagrenee M., *Corros. Sci.* 42 (2000) 127.
48. Labjar N., Lebrini M., Bentiss F., Chihib E.N., Hajjaji EL .S, Jama C., *Mater. Chem. Phys.* 119 (2010) 330.
49. Lebrini M., Lagrenee M., Traisnel M., Gengembre L., Vezin H., Bentiss F., *Appl. Surf. Sci.* 253 (2007) 9267.
50. Lagrenée M., Mernari B., Bouanis M., Traisnel M., Bentiss F., *Corros. Sci.* 44 (2002) 573.
51. Bentiss F., Lagrenee M., Traisnel M., Hornez J C., *Corros. Sci.* 41 (1999) 789,
52. Mc Cafferty E., Springer., *New York., Dordrecht., Heidelberg., London., New York,* 2010.
53. Tsuru T., Haruyama S., Gijutsu J.B., *Jpn.J., Soc. Corros. Eng.* 27 (1978) 573.
54. Afia L., Salghi R., Zarrouk A., Zarrok H., Benali O., Hammouti B., Al-Deyab S.S., Chakir A., Bazzi L., *Port. Electrochim. Acta* 30 (4) (2012) 267.
55. Oguzie E.E., *Corros. Sci.* 49 (2007) 1527 (35).
56. Martinez S., Stern I., *Appl. Surf. Sci.* 199 (2002) 83.
57. Hosseini S., Salari M.A., Ghasemi M., Abaszadeh M., *Z. Phys. Chem.*, 223 (2009) 769.
58. Bloom F. E., Kupfer D.J., (eds.) *Psychopharmacology: The Fourth Generation of Progress.* New York: Raven Press (1995).
59. Migahed M A., *Mater. Chem. Phys.* 93 (2005) 48.
60. Ahamad I., Prasad R., Quraishi M.A., *Corros. Sci.* 52 (2010) 933.
61. Noor E.A., Al-Moubaraki A.H., *Mater. Chem. Phys.* 110 (2008) 145.
62. Özcan M., Solmaz R., Kardas G., Dehri I., *Colloids Surf. A.* 325 (2008) 57.
63. Solmaz R., *Corros. Sci.* 52 (2010) 3321.
64. Döner A., Solmaz R., Özcan M., Kardas G., *Corros. Sci.* 53 (2011) 2902.
65. Moretti G., Guidi F., Grion G., *Corros. Sci.* 46 (2004) 387.
66. Fang J., Li J., *J. Mol. Struct.* 593 (2002) 179.
67. Amin A.M., Khaled F.K., Mohsen Q., Arida A.H., *Corros. Sci.* 52 (2010) 1684.
68. Zhang J., Liu J., Yu W., Yan Y., You L., Liu L., *Corros. Sci.* 52 (2010) 2059.
69. Li X., Deng S., Xie X., *J. Taiwan Inst. Chem. Eng.* 5 (4) (2014) 1865.
70. Li X., Deng S., Xie X., *Corros. Sci.*, 81 (2014) 162.
71. Lukovits I., Kalman E., et Zucchi F., *Corrosion*, 57 (1) 2001.
72. Parr G.R., Szentpaly L. v., et Liu S., *Am.J. Chem. Soc.* 121 (9) (1999) 1922.
73. Wazzan A.N., *Ind.J. Eng. Chem.* 26 (2015) 291.
74. Khaled F.K., El-Maghraby A., *Arab. J. Chem.* 7 (2014) 319.
75. Sasikumar Y., Adekunle S.A., Olasunkanmi O.L., Bahadur I, Baskar R., Kabanda M.M., Obot B.I., Ebenso E.E, *J. Mol. Liq.* 211 (2015) 105.
76. Hmamou D.B., Salghi R., Zarrouk A., Zarrok H., Touzani R., Hammouti B., et El Assyry A., *J. Environ. Chem. Eng.* 3 (2015) 2031.

(2017) ; <http://www.jmaterenvironsci.com>